Available online at www.sciencedirect.com

SciVerse ScienceDirect

Ceramics International 39 (2013) 4985–4990

CERAMICS INTERNATIONAL

www.elsevier.com/locate/ceramint

Studies on sintering kinetics and correlation with the sinterability of 8Y zirconia ceramics based on the dilatometric shrinkage curves

K. Rajeswari[a], S. Padhi[b], A.R.S. Reddy[a], Roy Johnson[a], Dibakar Das[c,*]

[a]Centre for Ceramic Processing, International Advanced Research Centre for Powder Metallurgy and New Materials, Hyderabad 500005, India
[b]Advanced Centre for Research in High Energy Materials, University of Hyderabad, Hyderabad 500046, India
[c]School of Engineering Sciences and Technology, University of Hyderabad, Hyderabad 500046, India

Received 19 July 2012; received in revised form 20 November 2012; accepted 28 November 2012
Available online 23 December 2012

Abstract

Prediction of the dominant sintering mechanism and corresponding temperature regimes become important in arriving at the optimum sintering schedule of ceramics. The sintering kinetics of 8Y zirconia (8YSZ) submicron powders, with particle sizes ~205 nm, has been evaluated through, (i) constant rates of heating and (ii) master sintering curve (MSC) technique. Slip cast green 8YSZ compacts, close to 50% of the theoretical density, have been subjected to dilatometry, for recording the shrinkage behavior, at constant heating rates of 5, 10 and 20 °C/min. The kinetics of the corresponding sintering process has been evaluated by estimating and comparing the apparent activation energies (Q) from the constant heating rate technique, and MSC approach. The observed apparent activation energy (~350 kJ/mol) suggests grain-boundary diffusion to be the dominant mechanism in sintering of 8YSZ ceramics.

Keywords: A. Slip casting; B. Microstructure-final; C. Diffusion; D. ZrO_2

1. Introduction

8 mol% Yttria stabilized zirconia is the most commonly employed electrolyte material for solid oxide fuel cell application, because of its high oxygen ionic conductivity and chemical stability over a wide range of temperatures [1]. Mechanical and electrical properties of YSZ have been studied extensively and found to be dependent on the final density and microstructure. Considerable efforts have been made in recent years to study the processing, densification and microstructural refinement of this material. Sintering is a critical step in fabricating a part with required density and microstructure. Sintering mechanism and activation energy of sintering are important for predicting the kinetics of material transport and hence the microstructure evolution. Through computer simulation kinetic analysis of the material transport, during sintering, has been studied by many authors [2–4], which describes quantitatively the elementary process involved in diffusional mass transport during sintering. However, the analysis requires critical evaluation with respect to the specific case, when various mechanisms are simultaneously involved in sintering. It is well known that the sintering behavior and microstructure are affected not only by the starting particle sizes of the material but also by the sintering parameters. Understanding of the mechanism/s and corresponding temperature regimes become important in arriving at the optimum sintering schedule to control the microstructure with high relative density. This can be achieved (by avoiding temperature regions that result in excessive grain growth without much densification) by a faster heating followed by a relatively slower heating schedule that results in minimum grain growth. Pushrod dilatometers are frequently used to study the shrinkage behavior of the material as a function of temperature or time at constant heating rates. Such studies are useful in determining the kinetics of material transport

*Corresponding author. Tel.: +91 40 23134454.
E-mail addresses: dibakar1871@gmail.com, ddse@uohyd.ernet.in (D. Das).

0272-8842/$ - see front matter © 2012 Elsevier Ltd and Techna Group S.r.l. All rights reserved.
http://dx.doi.org/10.1016/j.ceramint.2012.11.095

and the dominant mechanism in sintering. The validity of the sintering models is confined mainly to the early stage of sintering in the conventional solid state sintering, which were developed decades ago by Coble [5], Young and Cutler [6], and Wang and Raj [2,7]. The literature data on sintering mechanisms and activation energies for sintering and diffusion are confusing in many cases. The theory of master sintering curve (MSC) provides a new insight into the sintering phenomena. Master Sintering Curve approach was originally introduced by Su and Johnson [8,9] based on the combined-stage sintering model [4]. MSC enables the prediction of the densification behavior with the help of minimum number of preliminary experiments on a given sample. The relative density and a master variable follow a unique relationship in sintering of ceramic using different heating rates. The master variable combines the effect of sintering temperature and time and is called "work of sintering". The MSC has successfully been applied to the sintering of CeO_2 [10], TiO_2 [11], micro and nano-sized ZnO [12], nano 3Y-TZP [13] and ThO_2 [14].

In the present work slip cast green compacts of submicron 8Y zirconia powder were subjected to dilatometry and the corresponding sintering process (in the dilatometric experiment) has been investigated by estimating the activation energies from two different sintering models, the Wang and Raj model and a modified MSC model. The estimated activation energies, obtained from the two methods, have been compared and the dominant sintering mechanism has been identified for the slip cast 8YSZ ceramics sintered at 1550 °C with no soaking (in dilatometer) at different constant heating rates of 5 °C/min, 10 °C/min, and 20 °C/min.

2. Experimental procedure

Commercially available 8 mol% yttria stabilized zirconia powder (TZ-8Y, Tosoh, Japan), with an average particle size of ~205 nm, was dispersed in aqueous medium to form slurries, with solid loading in the range of 55–65 wt%, using 1 wt% Darvan 821A (R.T. Vanderbilt Co., Inc., Norwalk, CT, USA) as the dispersant. The suspension was then milled for 6 h in a pot jar mill using polypropylene bottles and zirconia balls of 1 mm diameter with 1:1 charge to balls ratio. The optimized slurry, with respect to solid loading and rheological properties, was slip cast into circular discs of 10 mm diameter and 4 mm thickness in plaster of Paris mold with subsequent drying in controlled humidity conditions of 50 °C and 75% relative humidity. Green pellets with 50% of the theoretical density were subjected to sintering in a Netzsch 402C dilatometer from room temperature to 1550 °C with no soaking. The peak sintering temperature was reached at different constant heating rates of 5, 10 and 20 °C/min.

8YSZ slip cast samples, in separate experiments, were sintered at 1550 °C for 2 h by conventional ramp and hold sintering (CRH) method at different heating rates (5, 10, and 20 °C/min). The sintered samples were ceramographically polished and thermally etched at temperatures 50 °C lower than the peak sintering temperature and were subjected to microstructure analysis in a scanning electron microscope (Model: HITACHI S-3400N SEM).

3. Results and discussion

3.1. Shrinkage

Fig. 1 shows the time–temperature evolution of shrinkage (%) of the entire dilatometry data. No shrinkage is observed till 1100 °C for all the heating rates. Shrinkage starts at 1100 °C, increases with further increase in temperature and attains a steady state value at around 1500 °C for all the heating rates employed during dilatometry. For a particular temperature shrinkage is highest for the sample heated at 5 °C/min and least at 20 °C/min as shown in Fig. 2.

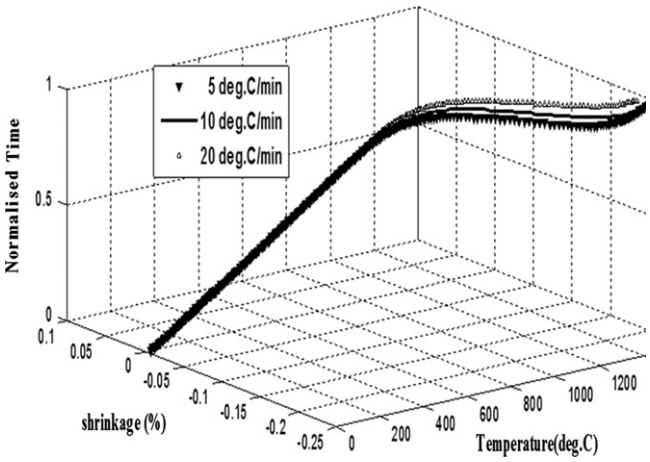

Fig. 1. The time–temperature evolution of the shrinkage (%) data of 8YSZ ceramics obtained from dilatometry.

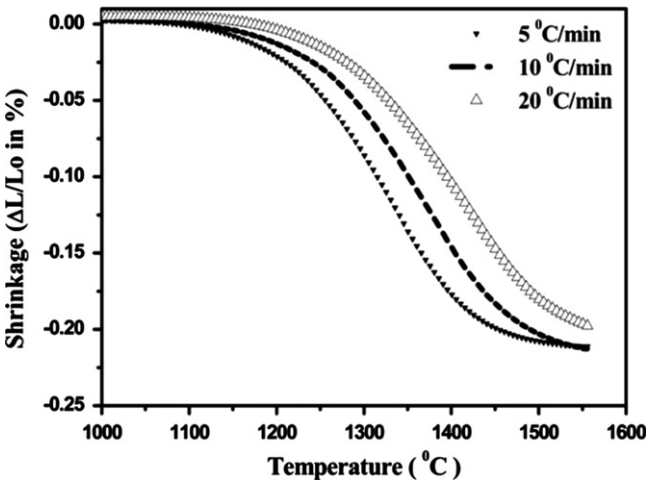

Fig. 2. Shrinkage behavior of 8YSZ ceramics as a function of temperature.

3.2. Microstructure

SEM micrographs of the 8YSZ samples, sintered at 1550 °C for 2 h by CRH method at different heating rates, are shown in Fig. 3(a–c). Fairly dense microstructures are observed with very few isolated pores here and there. The average grain size, measured by the line intercept method, is found to be around 7–8 μm. The dark spots in the microstructures are yttria segregation in the YSZ matrix as confirmed by the energy dispersive spectrometry (EDS) in the SEM analysis. The SEM micrograph of the sample, sintered at 1550 °C with no soaking and at a heating rate of 5 °C/min, is shown in Fig. 3(d) for comparison. The average grain size is smaller than that obtained from the 8YSZ sample sintered at the same peak temperature (1550 °C) and heating rate (5 °C/min) but soaked for 2 h (Fig. 3(a)). Few interconnected pores are still seen in the grain boundary regions. The effect of isothermal sintering (at 1550 °C for 2 h) is observed in Fig. 3(a). A microstructure with significant grain growth and few isolated pores in the matrix is obtained. In fact, 2 h soaking at the peak sintering temperature (1550 °C) has suppressed the effect of different heating rates (5, 10, and 20 °C/min) on the grain growth kinetics in sintering. However, the effect of soaking in the peak sintering temperature has not been considered in this investigation in determining the kinetics of sintering.

3.3. Estimation of activation energy by Wang and Raj method

This method was developed by Wang and Raj [2] for the estimation of activation energy at constant heating rates. In this method the equation for sintering rate can be separated into temperature-dependent, grain-size dependent and density-dependent quantities.

The mathematical form of the sintering rate equation is given by

$$\dot{\rho} = A\frac{e^{-Q/RT}}{T}\,\frac{f(\rho)}{d^n} \tag{1}$$

where T is the temperature, R is the universal gas constant, ρ is the instantaneous relative density of the sample, $f(\rho)$ is a density dependent function, $\rho(d\rho/dt)$ is the densification rate, Q is the activation energy, A is the pre-exponential factor, d is the grain size, and n is the grain size exponent ($=3$, when densification is controlled by lattice diffusion, and $=4$ by grain-boundary diffusion). The logarithm of Eq. (1) gives

$$\ln\left(T\dot{T}\frac{d\rho}{dT}\right) = -\frac{Q}{RT} + \ln[f(\rho)] + \ln A - n\ln d \tag{2}$$

where $\dot{T}$ is the heating rate which is held constant during the experiment. The plot of left hand side versus $1/T$ of Eq. (2) should give the value of Q provided that the data

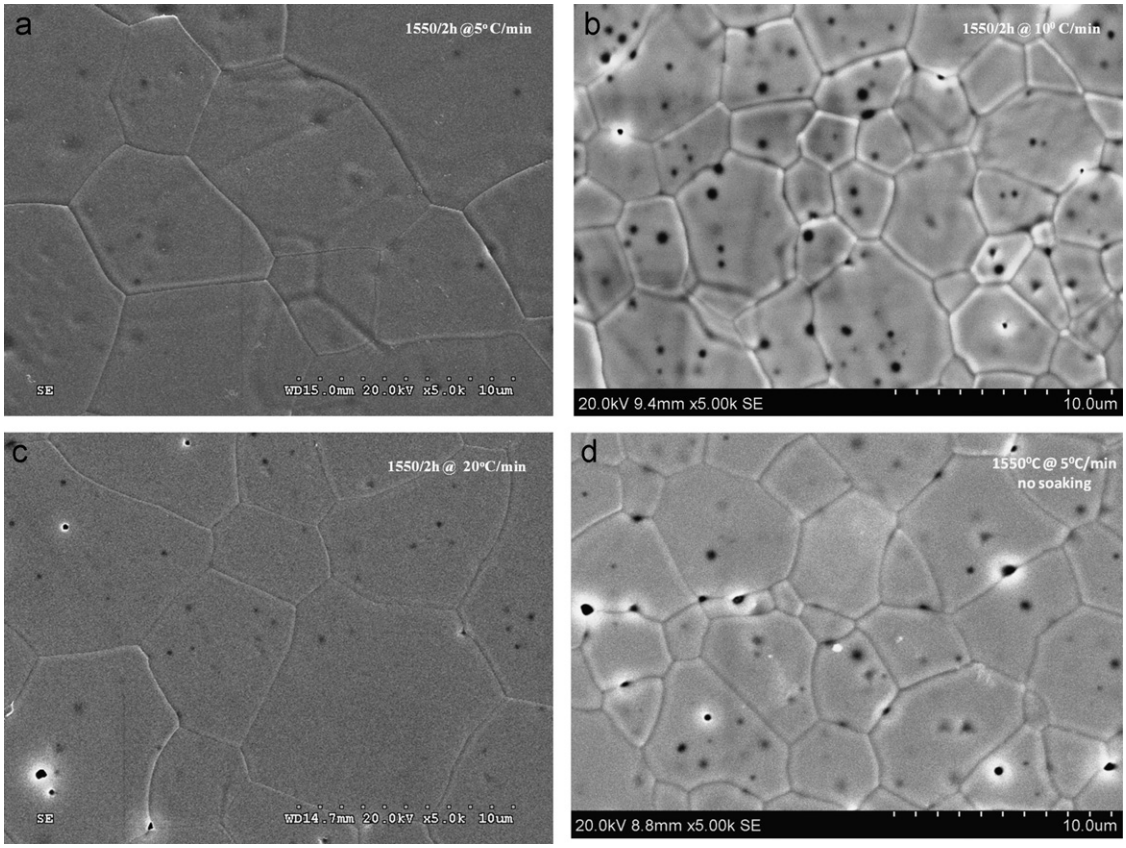

Fig. 3. Microstructure of 8YSZ samples sintered by the constant heating rate method at 1550 °C (a) for 2 h at heating rates of 5 °C/min, (b) for 2 h at heating rates of 10 °C/min, (c) for 2 h at heating rates of 20 °C/min and (d) without soaking at heating rates of 5 °C/min.

points are taken at constant values of ρ and d. The variation in d is eliminated by careful green state processing [15,16] of the sample. Data for constant value of ρ are obtained by changing the heating rates. The measurements lead to values of Q at different values of ρ.

The instantaneous relative densities of the samples were calculated from

$$\rho = \left(\frac{1}{1- \left|\Delta L/L_o\right|}\right)^3 \rho_o \quad (3)$$

where ρ is the relative density, $\left|\Delta L/L_o\right|$ is the absolute shrinkage in %, and ρ_o is the green density. The variation of instantaneous relative densities of the samples as a function of temperature is shown in Fig. 4. No change in relative density is observed up to 1150 °C for all heating rates. For temperatures beyond 1150 °C, the relative density increases with increase in temperature. Relative density is also seen to increase with decrease in heating rates at a particular temperature, a behavior observed similar to the shrinkage variation with temperature shown in Fig. 2. The densification rate ($d\rho/dt$) of the sample as a function of temperature is shown in Fig. 5 for all the heating rates. For all heating rates the densification rate increases with increase in temperature, attains a maxima and then decreases with further increase in temperatures. The peak in the densification curves shifts to the higher temperatures with increase in heating rates. Also, the densification rates decrease with increase in heating rates. The position and height of the densification curve are indicative of the activation energy of sintering of 8YSZ sample. In order to find the activation energy, the slopes of the curves in Fig. 4, at different values of relative densities, is measured. For each relative density, three values of $d\rho/dt$ at three different heating rates are obtained. These three values are plotted in an Arrhenius plot. The results are shown in Fig. 6 for five different values of relative densities ranging from 0.65 to 0.85. The activation energies for all relative densities were estimated from the slopes of these curves. The activation energy obtained from such estimation, 272–309 kJ/mol, is found to be in good agreement with that reported, 307 ± 10 kJ/mol, by Yeh and Sacks [17]. From a careful look at the plots in Fig. 6 it is seen that the lines for all relative densities (0.65–0.85) are strictly parallel to each other. In applying Eq. (2) on data shown in Fig. 4, to find out the activation energy (Q), it is assumed that no grain growth (coarsening) takes place during the intermediate stage ($\rho = 0.65$–0.90) of the sintering process. Grain growth at the intermediate stage is suppressed by improving the packing of the particles in the green state. For a green sample with uniform compaction the grain coarsening takes place in the final stage of sintering (relative density more than 90%, $\rho > 0.90$), when the nature of porosity changes from being open interconnected to closed and isolated [2]. In this investigation colloidal processing (slip casting) was adopted in processing the green 8YSZ samples to suppress coarsening in the intermediate stage, which could have led all the relative

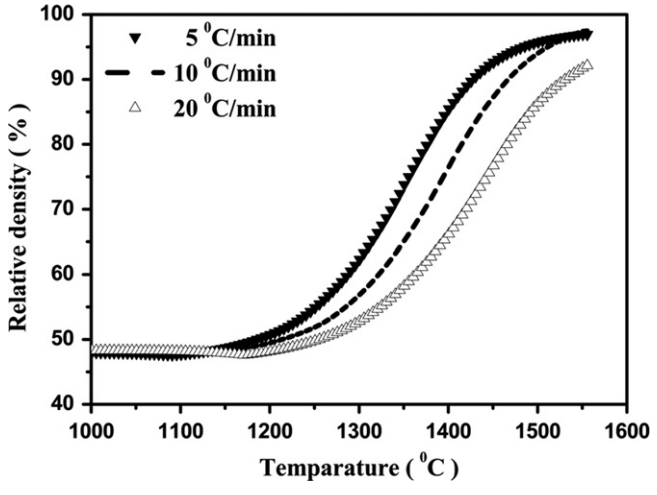

Fig. 4. Variation of relative density as a function of temperature for sintered 8YSZ samples (1550 °C without soaking).

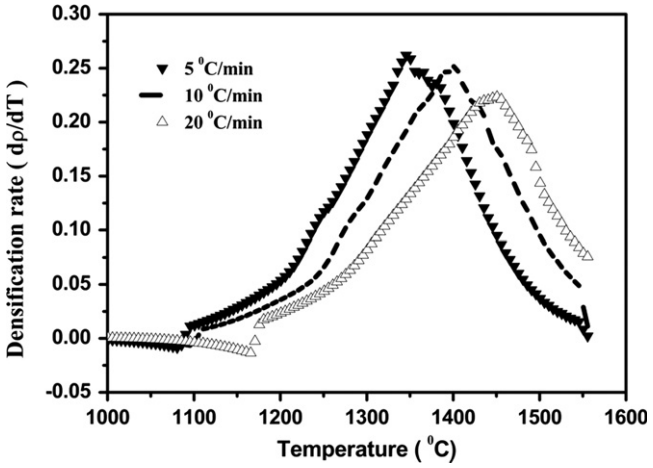

Fig. 5. Densification behavior of 8YSZ samples as a function of temperature.

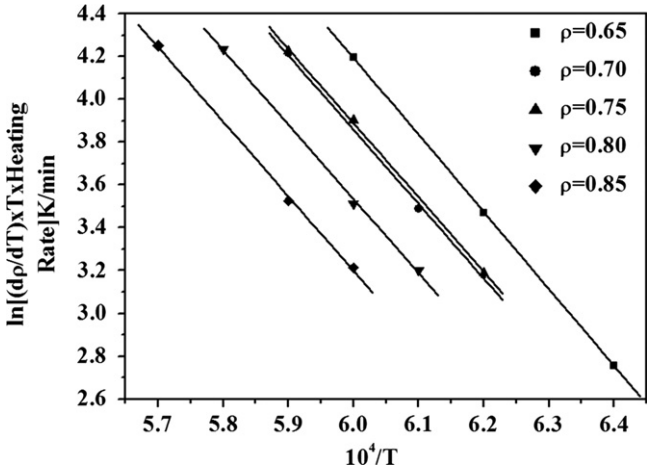

Fig. 6. Arrhenius plot, $\ln\left((d\rho/dt) \times T \times \dot{T}\right)$ versus $\left(10^4/T\right)$, of 8YSZ samples obtained from Wang and Raj method.

density lines (ρ=0.65–0.90) perfectly parallel to each other (single activation energy in the whole relative density range investigated). These data suggest the uniform compaction of the 8YSZ particle in the slip cast green sample.

3.4. Estimation of activation energy by the master sintering curve approach

The master sintering curve (MSC) [8,9,14] has been used to estimate the activation energy (Q kJ/mol) for densification. First, a Q value is assumed and the 'work of sintering' [8] for all the heating profiles (obtained from dilatometry) is computed using Eq. (4).

$$\boldsymbol{\Theta}(t, T(t)) = \int_0^t \frac{1}{T(t)} \exp\left(\frac{-Q}{RT(t)}\right) dt \tag{4}$$

where the parameter Θ is known as 'work of sintering' and depends only on sintering activation energy (Q) and time (instantaneous time in seconds; t) and temperature (T) profile of the dilatometry data. The integration in Eq. (4) has been evaluated by the trapezoidal rule and numerical integration [18] method. In this case a simple quantitative expression, Eq. (5), has been used to approximate the "work of sintering", which simultaneously accommodates the temperature and time evolution of the dilatometry data.

$$\boldsymbol{\Theta}(t,\ T(t)) = \frac{1}{2}\left\{\frac{1}{T(t)}\exp\left(\frac{-Q}{RT(t)}\right) + \frac{1}{T(t=0)}\exp\left(\frac{-Q}{RT(t=0)}\right)\right\}\Delta t \tag{5}$$

The expression in Eq. (5) provides with the "work of sintering" for the experimental dilatometry data without further division of domain of integration. The works of sintering for all the heating rates are taken as zero for the starting temperature (T=30.653 °C) of the dilatometry data. Δt is the time difference and R is the universal gas constant in Eq. (5).

The shrinkage curves obtained from the dilatometry experiments, at different heating rates (5, 10, 20 °C/min) are shown in Fig. 2. For all heating rates, the shrinkage starts around 1100 °C and attains a steady value at ~1500 °C. From the shrinkage curves relative densities are calculated using Eq. (3) and the relative density versus temperature plot is shown in Fig. 4. The important attributes of the plot shown in Fig. 4 are (i) the general shape of the curves is sigmoidal and the curves shift to higher temperatures with increasing heating rates and (ii) the maximum density is found to depend on the heating rates, the higher the heating rate lower is the sintered density.

The estimated relative density, from Eq. (3), are plotted against Log $\Theta(t,T(t))$, which represents the MSC for all heating rates. The data sets are fitted by a Boltzmann function, represented by Eq. (6), which is different from the standard fitting used in the literature [19].

$$\rho = \rho_f + \frac{\rho_i - \rho_f}{1+\exp\left(\text{Log}\,\boldsymbol{\Theta} - a/b\right)} \tag{6}$$

where a and b are fitting parameters, and ρ_i and ρ_f are the green and final sintered density respectively. The estimated ρ_f, calculated from Eq. (6), for the three heating rates (5, 10 and 20 °C/min) are 96.93%, 97.48% and 92.12%, respectively. If the correct value of Q is assumed all the data points should converge to a single sigmoidal curve. If they fail to converge, a new value of Q is chosen and the above steps are iterated until the apparent activation energy of sintering is obtained. The apparent activation energy of sintering is the minimum value of the mean residual squares (MRS; sum of residual squares divided by the total number of data points) in the MRS versus Q (chosen) plot. The residual squares have been calculated using Eq. (7) [20] over a set of 23 equally spaced relative density values (48%, 50%,…, 92%) in the shrinkage region of the dilatometry data.

$$(\text{Residual})^2 = \left\{\text{Log}\,\boldsymbol{\Theta}\left(\text{all rate}, \rho_{\text{fix}}\right) - \text{average}\left(\text{Log}\,\boldsymbol{\Theta}\left(\text{all rate}, \rho_{\text{fix}}\right)\right)\right\}^2 \tag{7}$$

where ρ_{fix} is the fixed value of relative density at which the residual is calculated. A total of 69 residual squares, obtained for a particular value of chosen Q, are averaged out. This gives the mean residual square (MRS) for that particular value of Q. Similar process has been repeated for all other chosen values of activation energies. The mean residual squares versus chosen values of Q are plotted in Fig. 7. The minimum of MRS comes out to be 0.0228 for Q=350 kJ/mol. This is the apparent activation energy of sintering and the corresponding MSC is shown in Fig. 8. The data points for all the three heating rates and the constructed MSC show good convergence. The estimated value of activation energy (350 kJ/mol) is within the range of activation energies (309–373 kJ/mol) reported in the literature for cubic zirconia [21,22]. The estimated

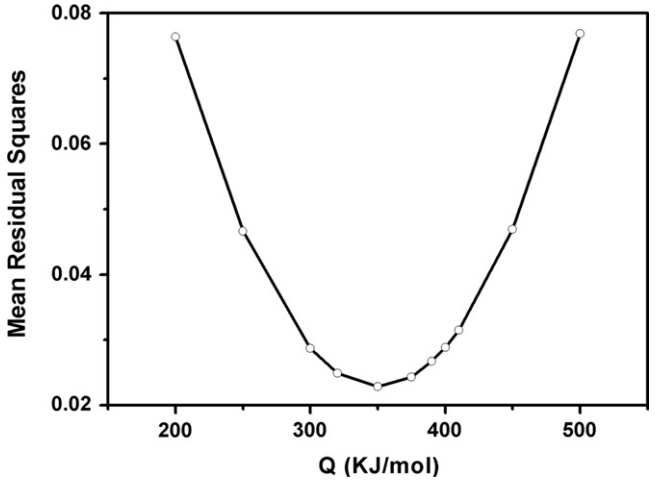

Fig. 7. Variation of mean residual square (MRS) with activation energy (Q) for 8YSZ samples.

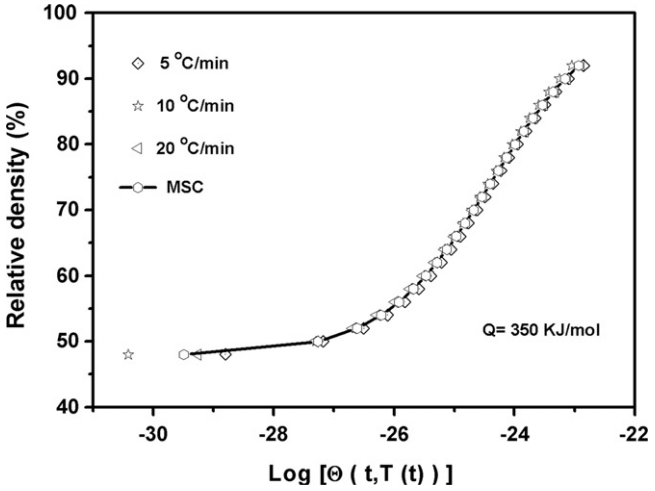

Fig. 8. Master sintering curve (MSC) of 8YSZ samples sintered at 1550 °C at constant heating rates of 5, 10, and 20 °C/min without soaking.

activation energy suggests grain-boundary diffusion (GBD) to be the dominant diffusional mass transport mechanism in the solid state sintering of 8YSZ ceramics.

4. Conclusions

The activation energy of sintering for 8YSZ ceramics has been estimated from the constant heating rate sintering by the Raj and Wang method and MSC approach. The estimated activation energy from the Wang and Raj method is $\sim 307 \pm 10$ kJ/mol in the relative density range 65–85%. The apparent activation energy of sintering, obtained from the MSC approach, for the entire shrinkage region (relative density of 48–92%) is found to be ~ 350 kJ/mol. The difference in activation energies, obtained from the two approaches, is probably due to the difference in the range of relative densities considered in this calculation. The estimated activation energy suggests grain-boundary diffusion (GBD) to be the dominant sintering mechanism in the early and intermediate stage of sintering of 8YSZ ceramics.

Acknowledgments

S. Padhi is thankful to Advanced Centre for Research in High Energy Materials (ACRHEM), University of Hyderabad for financial support. Help received from Dr. Surajit Dhara, School of Physics, University of Hyderabad, in analyzing the dilatometry data to construct the MSC is gratefully acknowledged.

References

[1] C.L. Robert, F. Ansart, C. Deloget, M. Gaudon, A. Rousset, Dense yttria stabilized zirconia: sintering and microstructure, Ceramics International 29 (2003) 151–158.

[2] J.D. Wang, R. Raj, Estimation of the activation energies for boundary diffusion from rate-controlled sintering of pure alumina, and alumina doped with zirconia or titania, Journal of the American Ceramic Society 73 (1990) 1172–1175.

[3] M.Y. Chu, M.N. Rahaman, L.C.D. Jonghe, R.J. Brook, Effect of heating rate on sintering and coarsening, Journal of the American Ceramic Society 74 (1991) 1217–1225.

[4] J.D. Hansen, R.P. Rusin, M.H. Teng, D.L. Johnson, Combined-stage sintering model, Journal of the American Ceramic Society 75 (1992) 1129–1135.

[5] R.L. Coble, Initial sintering of alumina and hematite, Journal of the American Ceramic Society 41 (1958) 55–62.

[6] W.S. Young, I.B. Cutler, Initial sintering with constant rates of heating, Journal of the American Ceramic Society 53 (1970) 659–663.

[7] J.D. Wang, R. Raj, Activation-energy for the sintering of 2-phase alumina zirconia ceramics, Journal of the American Ceramic Society 74 (1991) 1959–1963.

[8] H. Su, D.L. Johnson, Master sintering curve: a practical approach to sintering, Journal of the American Ceramic Society 79 (1996) 3211–3217.

[9] H. Su, D.L. Johnson, A practical approach to sintering, American Ceramic Society Bulletin 76 (1997) 72–76.

[10] D.Z.D. Florio, V. Esposito, E. Traversa, R. Muccillo, F.C. Fonseca, Master sintering curve for Gd-doped CeO_2 solid electrolytes, Journal of Thermal Analysis and Calorimetry 97 (2009) 143–147.

[11] D. Li, S. Chen, W.Q. Shao, X.H. Ge, Y.H. Zhang, S.S. Zhang, Densification evolution of TiO_2 ceramics during sintering based on the master sintering curve theory, Materials Letters 62 (2008) 849–851.

[12] K.G. Ewsuk, D.T. Ellerby, C.B. DiAntonio, Analysis of nanocrystalline and microcrystalline ZnO sintering using master sintering curves, Journal of the American Ceramic Society 89 (2006) 2003–2009.

[13] M. Mazaheri, A. Simchi, M. Dourandish, F.G. Fard, Master sintering curves of a nanoscale 3Y-TZP powder compacts, Ceramics International 35 (2009) 547–554.

[14] T.R.G. Kutty, K.B. Khan, P.V. Hegde, J. Banerjee, A.K. Sengupta, S. Majumdar, H.S. Kamath, Development of a master sintering curve for ThO_2, Journal of Nuclear Materials 327 (2004) 211–219.

[15] D.L. Johnson, Finding and utilizing the master sintering curve, Presented at Sintering, Pennsylvania, USA, 2003.

[16] C.P. Cameron, R. Raj, Grain growth transition during sintering of colloidal prepared alumina powder compacts, Journal of the American Ceramic Society 71 (1988) 1031–1035.

[17] T.S. Yeh, M.D. Sacks, Effect of particle size distribution on the sintering of alumina, Journal of the American Ceramic Society 71 (1988) C484–C487.

[18] M. Rathbone, R. Freer, Microwave-assisted sintering of ZrO_2–8mol% Y_2O_3: enhancement of densification, Ceramic Transactions 94 (1999) 45–55.

[19] C. Blaine, D. Gurosik, Seong Jin Park, M. German, F. Heaney, Master sintering curve concepts as applied to the sintering of molybdenum, Metallurgical and Materials Transactions A 37 (2006) 715–720.

[20] D.C. Blaine, S.J. Park, R.M. German, Linearization of master sintering curve, Journal of the American Ceramic Society 92 (2009) 1403–1409.

[21] C.B. DiAntonio, K.G. Ewsuk, D. Bencoe, Extension of master sintering curve theory to organic decomposition, Journal of the American Ceramic Society 88 (2005) 2722–2728.

[22] M. Kilo, G. Borchardt, B. Lesage, O. Kaitasov, S. Weber, S. Scherrer, Cation transport in yttria stabilized cubic zirconia: Zr tracer diffusion in $(Zr_xY_{1-x})O_{2-x/2}$ single crystals with $0.15 \leq x \leq 0.48$, Journal of the European Ceramic Society 20 (2000) 2069–2077.